Annealing helicase HARP closes RPA-stabilized DNA bubbles non-processively

Burnham, Daniel R.; Nijholt, Bas; De Vlaminck, Iwijn; Quan, Jinhua; Yusufzai, Timur; Dekker, Cees

DOI
10.1093/nar/gkx147

Publication date
2017

Document Version
Final published version

Published in
Nucleic Acids Research

Published online 28 February 2017

Nucleic Acids Research, 2017, Vol. 45, No. 8 ***4687–4695***
doi: 10.1093/nar/gkx147

Annealing helicase HARP closes RPA-stabilized DNA bubbles non-processively

Daniel R. Burnham[1], Bas Nijholt[1], Iwijn De Vlaminck[1], Jinhua Quan[2], Timur Yusufzai[2] and Cees Dekker[1,*]

[1]Department of Bionanoscience, Kavli Institute of Nanoscience, Delft University of Technology, Delft, 2629 HZ, The Netherlands and [2]Biological Chemistry and Molecular Pharmacology, Harvard Medical School, Boston, MA 02215, USA

Received October 12, 2016; Revised January 23, 2017; Editorial Decision February 20, 2017; Accepted February 27, 2017

ABSTRACT

We investigate the mechanistic nature of the Snf2 family protein HARP, mutations of which are responsible for Schimke immuno-osseous dysplasia. Using a single-molecule magnetic tweezers assay, we construct RPA-stabilized DNA bubbles within torsionally constrained DNA to investigate the annealing action of HARP on a physiologically relevant substrate. We find that HARP closes RPA-stabilized bubbles in a slow reaction, taking on the order of tens of minutes for ∼600 bp of DNA to be re-annealed. The data indicate that DNA re-anneals through the removal of RPA, which is observed as clear steps in the bubble-closing traces. The dependence of the closing rate on both ionic strength and HARP concentration indicates that removal of RPA occurs via an association-dissociation mechanism where HARP does not remain associated with the DNA. The enzyme exhibits classical Michaelis–Menten kinetics and acts cooperatively with a Hill coefficient of 3 ± 1. Our work also allows the determination of some important features of RPA-bubble structures at low supercoiling, including the existence of multiple bubbles and that RPA molecules are mis-registered on the two strands.

INTRODUCTION

Unwinding of dsDNA is ubiquitous in the cell, occurring during transcription, replication and repair (1), leading to a prevalence of negative supercoiling of DNA in cells (2,3). Under physiological values of applied force and torque, these negatively supercoiled DNA domains have a propensity to spontaneously form bubbles (4). These can be stabilized by the single-stranded-binding proteins such as replication protein A (RPA) which subsequently may affect DNA processing (5). RPA, the most abundant single-stranded-binding protein in mammalian cells (6), consists of three subunits (7) and four binding domains that enable an unstable 8 nt, and a stable 30 nt binding mode (8). It is heavily involved in replication, repair and recombination to protect and stabilize DNA.

Hep-A related protein, HARP, also known as SMARCAL1 (SWI/SNF-related, matrix-associated, actin-dependent regulator of chromatin, subfamily a-like 1), has the uncommon ability to re-anneal RPA-stabilized DNA bubbles into double-stranded DNA (9) via adenosine triphosphate (ATP) hydrolysis. It has been termed an annealing helicase because it has the reverse action of helicases that more commonly unwind DNA and allow single-stranded binding protein to bind ssDNA. It has been shown that HARP is recruited to sites of DNA damage *in vivo* (10) by RPA, and it is thought that HARP has a role in replication fork restart and repair (11–13).

HARP is a member of the helicase superfamily 2 (SF2) due to the amino acid-sequence similarity of seven helicase motifs (14). Furthermore, with its helicase-like region similar to the primary sequence of *Saccharomyces cerevisiae* Snf2p, it belongs to the Snf2 family (14,15). Despite the presence of these helicase motifs, no Snf2 protein has been shown to exhibit helicase-like activity (15,16). The Snf2 family consists of ATP-hydrolyzing proteins and they have been identified in eukaryotes, eubacteria, and archea (14,15). Some proteins within the family act as ATP-dependent DNA translocases, while others have been shown to generate torsion within DNA (17) or to affect other DNA–protein interactions (14).

Only a handful of proteins have been shown to have the ability to rewind DNA, including RecG and UvsW (18). Even fewer have been shown to anneal RPA-stabilized DNA bubbles, with HARP and ZRANB3 (AH2) the only two to have been reported to do so (19). Mutations in HARP are responsible for Schimke immuno-osseous dys-

*To whom correspondence should be addressed. Tel: +31 15 27 86094; Fax: +31 15 27 81202; Email: c.dekker@tudelft.nl
Present addresses:
Daniel R. Burnham, The Francis Crick Institute, 1 Midland Road, London, NW1 1AT, UK.
Iwijn De Vlaminck, Nancy E. and Peter C. Meinig School of Biomedical Engineering, Cornell University, Weill Hall Ithaca, NY 14853, USA.

plasia, a severe autosomal-recessive pleiotropic disorder (20). In this work, we aim to elucidate the mechanism through which HARP interacts with RPA in order to anneal RPA-stabilized DNA bubbles (9).

With the high affinity for fork DNA (9,12) and known interaction with RPA (10,21), the ideal single-molecule substrate to study HARP is a ds/ssDNA junction where the ssDNA is bound by RPA, and yet the molecule retains torsional constraint. Indeed, our approach creates such a physiologically relevant structure by forming an RPA-stabilized bubble within a single molecule of dsDNA through binding of RPA to a negatively supercoiled dsDNA molecule (22). The single-molecule tool of choice here, magnetic tweezers (MT), allows the well controlled application of torque and the creation of supercoiling. By carefully tuning the force applied to the DNA, writhe that is produced upon supercoiling is transferred into plectonemes. Each time an additional helical turn is placed into the DNA ∼180 bp are formed into a loop that no longer contributes to the end-to-end length of the DNA. Any small change in the hybridized state (hence linking number) of the DNA alters the number of helical turns present in torsionally constrained molecules and, in doing so forms or removes plectonemic loops, which in turn decreases or increases the DNA end-to-end length. As RPA binds to DNA to form our bubble substrate, it 'unwinds' regions which causes a local change in linking number that must be balanced as the total linking number is conserved. This balance is realized by the creation or removal of plectonemes, and hence a large, detectable addition or subtraction of 160 bp to the DNA length. Having created an RPA-stabilized DNA bubble, the action of HARP should be directly observable in real time, as it re-anneals the substrate and hence induces sizeable DNA length changes.

Here, we demonstrate that we are able to observe, for the first time, the annealing of RPA-stabilized bubbles by HARP in real time. From the comprehensive set of data, we propose a mechanism for the observed low processivity of HARP annealing, and establish previously unknown details about the structure of RPA bubbles at physiologically relevant supercoiling ($\sigma \lesssim -0.03$) (23).

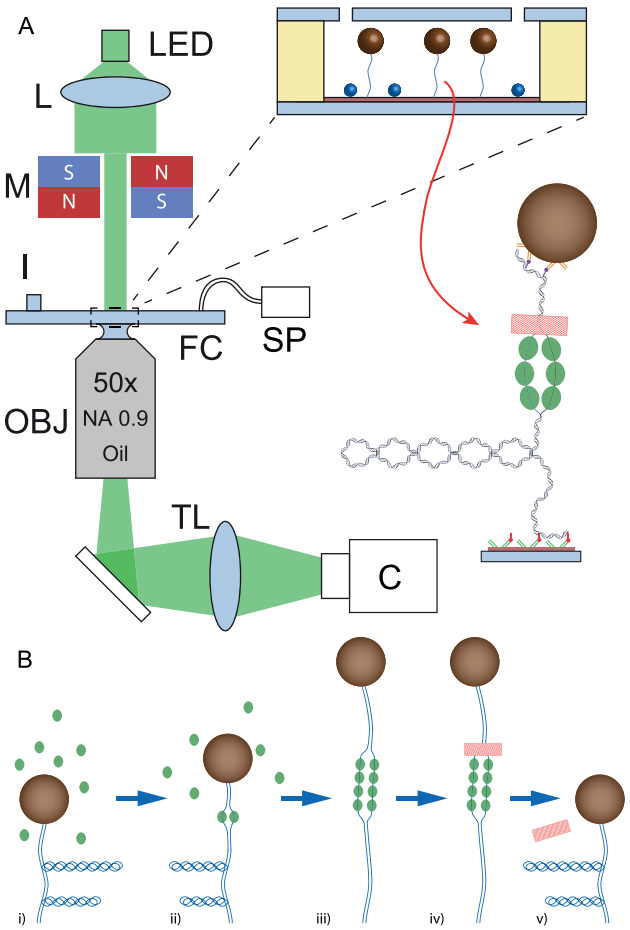

Figure 1. Magnetic tweezers apparatus used in this study and outline of assay, (i–v). (**A**) An LED provides illumination via a collimating aspheric lens, L, through magnet assembly M. The flow cell is imaged via a 50× objective in conjunction with an achromatic doublet tube lens, TL, onto a CMOS camera. Sample is pipetted into the inlet, I, and removed via syringe pump, SP. (**B**) (i) Sequence of events in the experiment. DNA is supercoiled by applying positive rotations to the bead with, resulting in the formation of plectonemes; and RPA is added. (ii) The supercoiling is switched to negative values, enabling the start of a torsionally regulated RPA-binding reaction. (iii) Once all writhe has been removed from the DNA, RPA binding ceases. (iv) All remaining non-bound RPA is removed from the flow cell and HARP is placed in the flow cell in the desired concentration and buffer conditions. (v) Any action that HARP performs that effects the annealed state of the DNA will result in a change in the number of plectonemes. As reported in this paper HARP closes the RPA-stabilized bubble, reforming the natural helical structure, thus creating 'negative' plectonemes and hence the microsphere will decrease in height.

Single-molecule setup

Our assay employs single-molecule MT that allow the application of both force and torque on a superparamagnetic microsphere. By tethering a dsDNA molecule between a glass surface and the microsphere, constraining both strands of the DNA duplex to the respective surfaces, magnet rotations are able to over- or underwind the DNA. Indeed, through applying magnet rotations against the helical nature of the DNA, negative supercoiling can be imparted.

It is generally assumed that negatively supercoiled DNA contains 'bubbles', local areas where the DNA duplex has 'melted' into two single strands. The propensity and size of such bubbles depends on force (24), although little is known about their stability, size or lifetime. We apply relatively low forces such that creation of DNA bubbles creates a significant DNA extension change via a change in plectoneme number. Any bubble that is formed is likely transient (25), and to prevent re-hybridization we use single-stranded-binding protein, namely RPA, resulting in a permanently open structure.

Figure 1(i–v) shows the design of our assay (See 'Materials and Methods' section for details). Once tethered and suitable DNA molecules are identified, the magnetic microspheres are held at a force of ∼0.5 pN and rotated about the z-axis in the same sense as the natural helical twist of the DNA, resulting in the creation of positive plectonemes (26). RPA is then placed in the flow cell at the desired concentration. No reaction takes place as no binding substrate is available for the single-stranded-binding protein due to the overtwisting of the DNA (4) (Figure 1(i)). The mag-

nets are then rotated such that the DNA is twisted against the natural helical twist resulting in negatively supercoiled (plectonemic) DNA that has a propensity to form transient bubbles large enough to initiate torsionally regulated RPA binding (Figure 1(ii)) (4,27). Each RPA molecule that stably binds to the DNA has a footprint of 30 nt (7,27) and hence removes about three helical turns from the dsDNA, creating a local decrease in linking number of −3. In order to conserve linking number globally, three plectoneme loops are removed as a result, which is observed as a clear increase in the microsphere height. Once all writhe has been removed from the DNA, RPA binding is no longer possible (Figure 1(iii)). Next, all remaining non-bound RPA is removed from the flow cell, and HARP is placed in the flow cell at the desired concentration and buffer conditions (Figure 1(iv)). The hypothesis is HARP will now re-wind RPA-stabilized bubbles in a highly processive manner (9,13), reforming the natural helical structure. In order to again conserve linking number, negative plectonemes will re-appear and hence the microsphere will decrease in height (Figure 1(v)).

MATERIALS AND METHODS

DNA constructs

A 21 kb construct was created through growing up a 'pSuperCos-lambda1,2' custom plasmid in bacteria. This was created by cloning two Lambda DNA fragments into pSuperCos. The first lambda fragment was created using polymerase chain reaction (PCR) on the region 39 017–48 413 with forward primer AAGGAAAAAAGCGGCCGC TACATCTCGAGATGGTGCATCCCTCAAAACGAG and reverse primer GGAAAGGGCCCGTAAAGTGA TAATGATTATCATC before being digested with NotI (12) and PspOMI (9476) and inserted into lambda DNA with NotI at positions 8 and 59. The second lambda fragment was created using PCR on the region 22 502–27 465 with forward primer TTGGCGCGCTTGATAC ATCAACTGCACCTGATATTG and reverse primer CCAGATCTACGACCTGCATAACCAGTAAG and inserted into the former step using BglII (12027) and BssHII (12 588). The resulting plasmid is 20 678 bp in length. A biotin handle was made using PCR on pBluescriptII SK+ (Stratagene) with forward primer GACCGAGATAGGGTTGAGTG and reverse primer CAGGGTCGGAACAGGAGAGC. The PCR reaction contains 0.2 mM dNTPs (Promega) and 0.04 mM biotin-16-dUTP (Roche Diagnostics). This handle, with approximately one out of every five thymine nucleotides replaced by a biotin-16-dUTP, was digested with XholI giving a biotin-handle of either 554 or 684 bp. To create a digoxigenin handle, the same procedure was performed except using dig-11-UTP and digestion with NotI to give a digoxigenin-handle of 614 or 624 bp. After digestion these handles are ligated onto the digested (Xhol and NotI) pSuperCos-lambda1,2 to form the final construct.

HARP preparation, buffers and reagents

HARP and RPA was prepared and purified following the procedure of Yusufzai and Kadonaga 2008 (9). HARP buffer (HB) consisted of 10 mM Tris pH 7.5, 16.8 mM KCl, unless indicated otherwise, 1.68 mM $MgCl_2$, 0.98 ethylenediaminetetraacetic acid (EDTA), 1.5 mM ATP unless indicated otherwise and 0.5 mM dithiothreitol. The dithiothreitol is made fresh from dry stock on the day of each experiment. RPA buffer (RB) consisted of 30 mM Tris pH 7.5 and 16.8 mM NaCl.

Magnetic tweezers

MT were used as extensively described before (28). A multiplexed MT system was employed (29) with the important details described below and in Figure 1. The system is based on a custom built microscope utilizing a 50× Plan NA 0.90 Oil (Nikon) with an achromatic doublet tube lens (200 mm) to provide 50× magnification. Illumination is provided from a green LED that, once collimated with an aspheric lens, is projected through the magnet assembly onto the flow cell. The magnet assembly holds two 5 mm cubed NdFeB magnets (W-05-N50-G, Supermagnete, Germany) in the vertical orientation (30) with vertical and angular position controlled by high-resolution translation and rotation stages (M-126.PD1, C-150.PD, Physik Instrumente, Germany). The image is focused onto a CMOS camera (Falcon 1.4M, Teledyne Dalsa, Germany) with images used directly for real time tracking via custom LabVIEW (National Instruments) code for immediate feedback. Compressed images are saved to disk for post processing and multiplexed microsphere tracking (29,31). The flow cell is constructed from two type-one coverslips (BB024060S1, Fisher Scientific, Netherlands), where one coverslip was sandblasted to create two 3-mm holes for flow inlet and outlet. Both coverslips are placed in an ultrasonic acetone bath for 30 min before being washed in isopropanol and left to dry. The bottom coverslip is first coated in a 1 in 400 ethanol (v/v) diluted solution of polystyrene microspheres (Polysciences Europe GmbH, Germany) and heated on an 80°C hotplate for 15 s, to later act as reference microspheres. Next, the same coverslip is coated in 0.1% w/v nitrocellulose (LC2001, Invitrogen, USA) and heated on an 80°C hotplate until dry. Finally, a two-ply piece of paraffin wax film (Parafilm M, Bemis, USA) is sandwiched between the two coverslips and heated on an 80°C hotplate for 60 s while providing gentle pressure to ensure sealing. The constructed flow cells can be kept at 4°C for up to two months, until experiments are conducted.

Tethering of DNA-microsphere constructs

Approximately 100 μl of anti-digoxigenin (Fab fragments 11214667001, Roche Diagnostics, Netherlands) (100 $\mu g ml^{-1}$) is pipetted into a flow cell via capillary action and left at room temperature for 30 min. Next the anti-digoxigenin is replaced with 1 ml of $T_{20}E_5$ (20 mM Tris pH 7.5 (Promega, H5123), 5 mM EDTA (Sigma-Aldrich, E7889)) before being replaced by bovine serum albuemin, bovine serum albumin (BSA) (100 mg ml^{-1}) (B9001S, Bioke, Netherlands) for 1 h before finally being replaced by $T_{20}E_5$ and mounted in the apparatus. To bind DNA constructs to magnetic microspheres, 5 μl of 1 μm diameter magnetic microspheres (Dynabeads MyOne Streptavidin C1, Life Technologies) are washed in 100 μl of $T_{20}E_5$

+ $Tween_{0.05}$ (0.05% v/v Tween 20 (Promega, H5151)) before being aggregated with a magnet in order to remove the supernatant. This is repeated three times before re-suspension in 10 μl $T_{20}E_5$ + $Tween_{0.05}$. A total of 1 μl of DNA stock solution is added to the washed microspheres at a concentration such that the molar ratio of microspheres and DNA is ∼1 : 1. The volume of DNA added is adjusted in order to optimize the number and quality of tethers in the field of view. The DNA and microspheres are left at room temperature for 20 min. The constructs are washed a final time with 59 μl of $T_{20}E_5$ + $Tween_{0.05}$ and 1 μl BSA, aggregated using a magnet and supernatant removed. Finally the constructs are re-suspended in ∼200 μl of $T_{20}E_5$ + $Tween_{0.05}$. This final volume is also adjusted in order to optimize the number and quality of tethers in the field of view. Tethers are created by flowing approximately 100 μl of the microsphere-DNA construct suspension into the flow cell before stopping all flow from the syringe pump and leaving the microsphere-DNA constructs for 10 min. Finally ≥1 ml of $T_{20}E_5$ is flowed through the flow cell to remove any non-tethered microspheres and DNA.

Details of MT assay

Once tethered, the DNAs are characterized by performing a dynamic force-extension curve (29,32), recording motion at a fixed magnet height to calibrate forces (32) and rotating the magnet from 0 to +80 to −80, and back to 0 turns, at 0.45 ± 0.01 pN first in HB and secondly RB to measure rotation curves. These curves allow the calculation of any rotation offset due to ionic strength variation, that will affect the amount of supercoiling for each tether. Any tethers that were found to have the incorrect mechanical parameters or that were not torsionally constrained were rejected from analysis. The flow cell is then flushed to contain RB, and the force is set to 0.45 ± 0.01 pN and the agents are rotated to +40 turns ($\sigma = 0.02$) at 4 Hz. Next a 200 μl, 2.2 μM stock solution of RPA is removed from a −80°C freezer, defrosted in a room temperature water bath and a 10 nM solution of RPA in RB is pipetted into the flow cell. Finally, the reaction is started by rotating the magnets to −60 turns ($\sigma = -0.03$) at 20 Hz. Once the reaction appears to be finished (as seen by microsphere height returning to that of non-supercoiled DNA) the force is increased to 0.70 ± 0.02 pN as a secondary measure to ensure the reaction has completed as the rate is force dependent (27). Next, 5 ml (∼50× the flow cell volume) of HB is flushed through the flow cell in order to remove all non bound RPA. The force is then changed to 0.45 ± 0.01 pN. Finally a 10 μl, 1.415 μM stock solution of HARP is removed from a −80°C freezer, defrosted in a room temperature water bath and the desired concentration of HARP in HB is prepared and immediately pipetted into the flow cell. The position of the probe and reference microspheres are tracked using a quadrant-interpolation algorithm (31) from the stored images after the experiments were completed. All data was recorded at a frame rate of 50 Hz, with an exposure time of 20 ms for each frame.

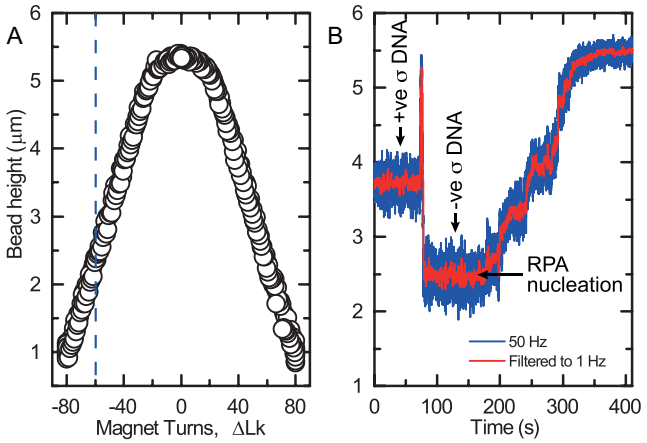

Figure 2. Rotation curve and RPA-stabilized bubble formation. (**A**) Change in DNA tethered microsphere height as a function of magnet rotations or linking number, ΔLk, attributed to plectoneme formation at 0.45 ± 0.01 pN. The addition or removal of a plectoneme results in a predictable height change of 62 ± 1 nm, and the binding or dissociation of a single RPA results in a 187 ± 4 nm height change. This occurs at constant ΔLk (dashed blue line) due to torsional constraint on the molecule. (**B**) A representative example of RPA binding to a single DNA tether at 0.45 ± 0.01 pN and RPA concentration of 10 nM. The initial microsphere height indicates positive supercoiling due to +40 magnet turns. The spike in height is due to magnet rotations at 20 Hz against the natural helical twist of DNA until −60 magnet turns are reached and hence a lower microsphere height is observed. After ∼100 s an RPA nucleation event occurs and binding continues until the microsphere reaches the same height as bare DNA with zero supercoiling, except here the supercoiling is negative with magnet turns remaining at −60. Raw data are at 50 Hz; red overlaid line is data filtered to 1 Hz.

RESULTS AND DISCUSSION

To understand the detected signals, which are variations in microsphere height, it is useful to examine a 'rotation curve' (Figure 2A), which describes how the microsphere height varies as a function of applied magnet rotations or linking number, ΔLk. At low force, the height decreases when applying rotations, due to the formation of plectonemes. The addition or removal of a plectoneme results in a predictable height change of 62 ± 1 nm, measured from the gradient of the rotation curve in Figure 2A. Consequently the binding or dissociation of a single RPA, with 30 nt footprint, associated with three plectonemes, will result in a 187 ± 4 nm height change. This all occurs at constant total linking number, due to the torsional constraint on the molecule. The changing height along the line of constant supercoiling (blue dashed line in Figure 2A), indicates where the signal is obtained.

Displayed in Figure 2B is a representative example of RPA binding to a single DNA tether. The initial microsphere height indicates positive supercoiling due to +40 applied magnet turns, followed by a spike in height as the magnets are rotated at −20 Hz before reaching −60 magnet turns and hence a lower microsphere height is reached. After ∼100 s, nucleation of RPA binding occurs which continues until the microsphere reaches the same height as would be the case for bare DNA with zero supercoiling, except here the supercoiling is negative with the magnet turns remaining at −60.

HARP closes RPA-stabilized DNA bubbles at very low speed

Figure 3A shows a typical HARP activity trace, demonstrating the closing of an RPA-stabilized bubble. At the start of the trace the micosphere height is constant, indicating that the RPA bubble is stable (Supplementary Figure S1). After the addition of HARP, at the time indicated by the vertical blue line (which occurs through temporary loss of microsphere tracking) the microsphere height gradually decreases until it reaches the height expected for bare DNA that is unwound by −60 turns. In a control experiment in the absence of ATP, HARP had no activity (Supplementary Figure S2) as expected from previous work (9).

The usual spontaneous dissociation of RPA from DNA is both force and ionic strength dependent (27) but the inclusion of $MgCl_2$ in HB acts to completely stabilize the system, even in the most favorable of conditions (Supplementary Figure S1) (33). Therefore, any action observed can be solely attributed to the presence of HARP. The rate of DNA rewinding, while slow compared to some molecular motors, such as prokaryotic replicative helicases (34,35), fits in the regime observed for bacteriophage and eukaryotic replication machinery (36).

The rate of unwinding by helicases is proportional to force, with higher forces assisting the unwinding reaction (34,37). Given this well established behavior, it would be expected that an annealing helicase would be hindered by force, slowing down with increasing force. However, counterintuitively, we observe the rate of annealing to increase with force, Figure 3C. Furthermore previous single-molecule studies on the kinetics of RPA on DNA (27) show that in the absence of an annealing helicase, the effect of force is opposite to the effect observed here, in the presence of HARP. In the absence of HARP, the rate of reannealing decreases with increasing force; whereas conversely, in the presence of HARP, the rate of reannealing increases with force. This may be explained by the altered topology of the DNA (38) which is consistent with the proposal that binding of HARP to the fork produces a conformational change (13).

Elucidating the mechanism of HARP

One would expect that, with increasing monovalent salt, RPA is removed at a higher rate from DNA due to the increased electrostatic screening and as observed for spontaneous dissociation (27). However, as seen in Figure 3B the opposite trend is observed; the time taken for the DNA to re-hybridize increases with ionic strength. Together with the demonstrated high stability of the RPA bubble due to $MgCl_2$, this finding shows that increasing monovalent salt must alter the affinity of HARP for the DNA–RPA substrate. If a single HARP molecule performed the complete unwinding reaction, the rate would likely not alter with ionic strength. These data thus point towards a non-processive model where the rate of unwinding is governed by HARPs affinity for the substrate.

HARP observes Michaelis–Menten enzyme kinetics with $V_{max} = 0.99 \pm 0.02$ min^{-1} and $K_{max} = 0.016 \pm 0.002$ mM (Supplementary Figure S2). All experiments here are carried out at 1.5 mM ATP concentration and thus are not rate limited by ATP hydrolysis. Figure 3D displays the fraction

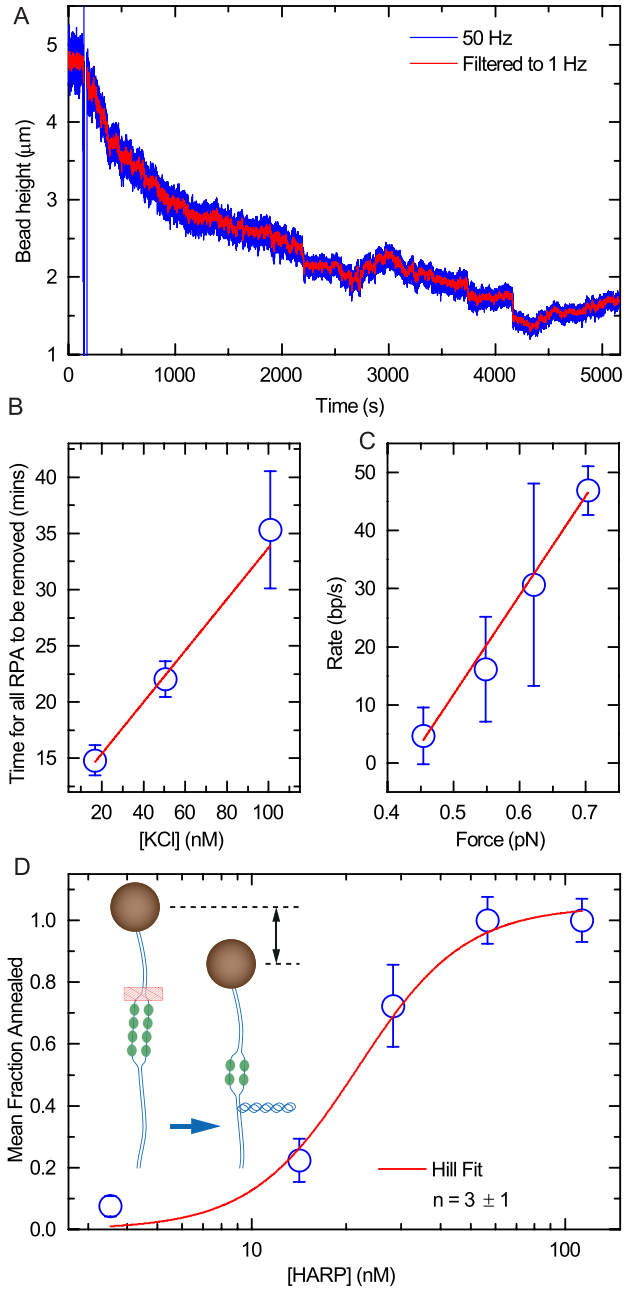

Figure 3. (**A**) Typical HARP activity trace demonstrating the closing of an RPA-stabilized bubble. Before the addition of 26 nM HARP, indicated by the vertical blue line (due to loss of microsphere tracking from flow), the RPA bubble is stable. After addition of HARP the microsphere goes down. KCl concentration is 101 mM. (**B**) An increase in ionic strength increases the time taken for the bubble to close. HARP concentration is 57 nM. Line is a guide to the eye. Error bars are sem; $n = 10$ (**C**). The rate of the annealing reaction increases as a function of applied force. Line is a guide to the eye. Error bars are sem; $n = 5, 11, 5, 4$ in order of increasing force. (**D**) The fraction of bubble closed as a function of HARP concentration shows, through a fit with the Hill equation, that HARP acts with positive cooperativity, requiring a minimum of 3 ± 1 HARP molecules to produce a functional effect. Error bars are sem; $n = 7, 12, 6, 10$ in order of increasing concentration. Data in panels were measured at a force of 0.45 ± 0.01 pN.

of bubble annealed as a function of HARP concentration. By treating the DNA–RPA bubble complex as the substrate, the data can be fit with the Hill equation to obtain a Hill coefficient of 3 ± 1, showing that HARP acts with positive cooperativity, requiring a minimum of 3 ± 1 HARP molecules to produce a functional effect (39). With the assay used here it cannot be determined if this cooperativity is a direct interaction or perhaps a long-range interaction where HARP acts at both ends of the bubble (13).

Discrete steps in microsphere height reveal microscopic information about RPA structures

The HARP-induced closing of RPA-stabilized bubbles exhibits discrete steps in microsphere height (Figure 4A), which we attribute to the removal of individual RPA molecules. As the reaction speed is much slower than the acquisition of microsphere position, the steps can be clearly determined and the details used to elucidate details about the RPA disassembly. To objectively analyze these steps, each trace was first filtered with an edge-preserving Chung–Kennedy algorithm (40) and subsequently a power spectrum of the pairwise difference distribution function of trace points was made for each DNA re-annealing trace. The step size is then taken as the inverse of the peak with the highest spatial frequency that lies above a 4δ threshold, where δ is the standard deviation of the power of the highest half of spatial frequencies (41). The same process was also carried out using a Savitzky–Golay filter (42) and similar results were obtained (Supplementary Figure S4).

The mean step size observed was 128 ± 10 nm with a distribution showing a broad peak between values of ∼75–175 nm, as displayed in Figure 4B. As estimated above, the dissociation of a single RPA molecule is expected to result in a step size of 187 ± 4 nm due to the addition of three plectoneme loops to the DNA. If pairs of RPA, i.e. those RPA molecules opposite to each other on the complementary DNA strands, were removed in unison, a sharp normal distribution around 187 ± 4 nm would thus be expected. However, the mean value and this broad distribution, biased towards smaller steps, must be explained by steps that are a fraction of the RPA footprint. This can only be the case if the RPA molecules are mis-registered along the two complementary ssDNA strands. Then it is possible to observe any step size up to a maximum of one full RPA removal. Indeed, the abundance of steps have a value below 200 nm.

Finally, we consider the time between each step in microsphere height, the dwell time. From Figure 4A it is already apparent that the dwell time increases as the reaction proceeds. This is quantified in Figure 4C, which indicates a consistent linear increase in dwell time at the beginning of the reaction, followed by a plateau of ∼280 s after ∼10 steps. We believe this to be another indication of the non-processive nature of the HARP-induced annealing. Note that the time to remove an RPA molecule should have no memory of the previous dwell time, no matter how RPA is distributed. However, the time that it takes for HARP to find a fork-RPA junction would increase as the number of reaction sites decreases, which is possible if multiple bubbles exist at the start of the reaction. The linear increase up to 10 steps thus suggests a lower limit of ∼5 bubbles exist at the

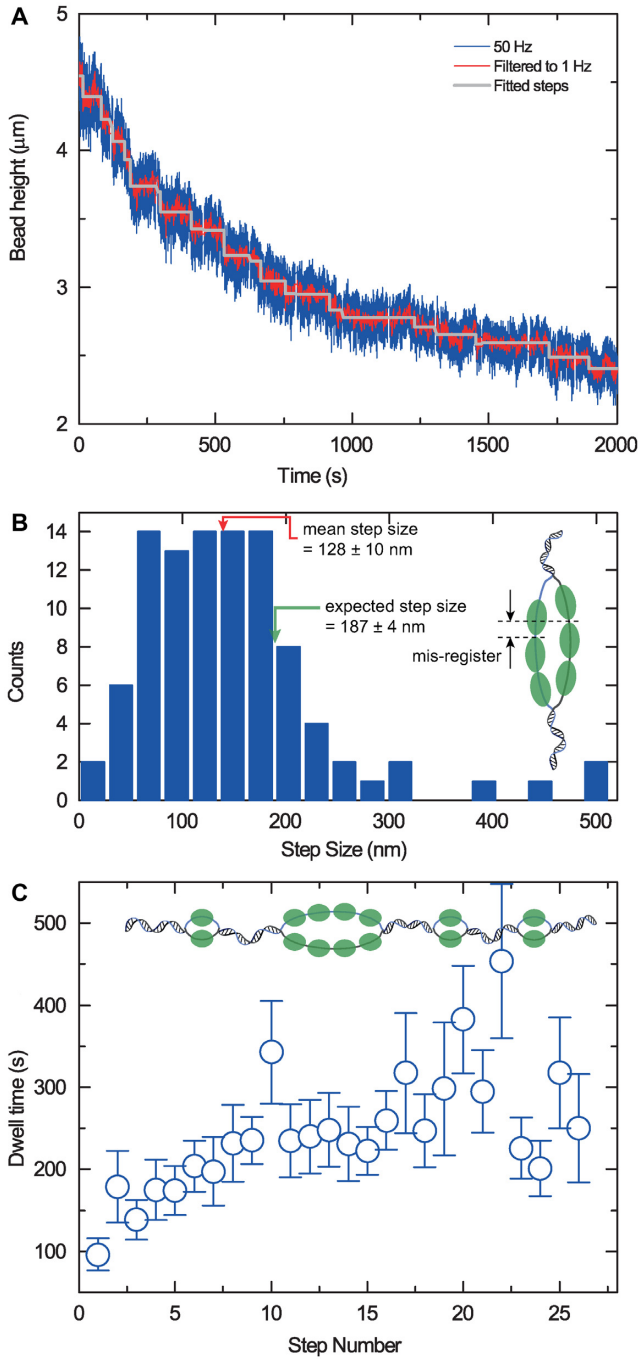

Figure 4. Data on step size and dwell time for bubble closure. (**A**) Typical HARP activity trace displaying steps in microsphere height during bubble closure. The fitted steps trace overlaid here are found using the technique of Kerssemakers *et al.* but all other step analysis is as described in the text (45). HARP concentration is 57 nM and KCl concentration is 101 mM (**B**) Histogram of step sizes that occur during closure of an RPA stabilized bubble. The mean step size (red arrow) observed is 128 ± 10 nm, lower than the expected 187 ± 4 nm, with a broad distribution that is biased towards smaller steps, indicating the RPA molecules are mis-registered along the homologous ssDNA strands (inset diagram). (**C**) Dwell time between RPA removals as the reaction proceeds. The initial linear increase at 1–10 steps indicates at least five separate bubbles exist. Error bars are sem; $n = 6$.

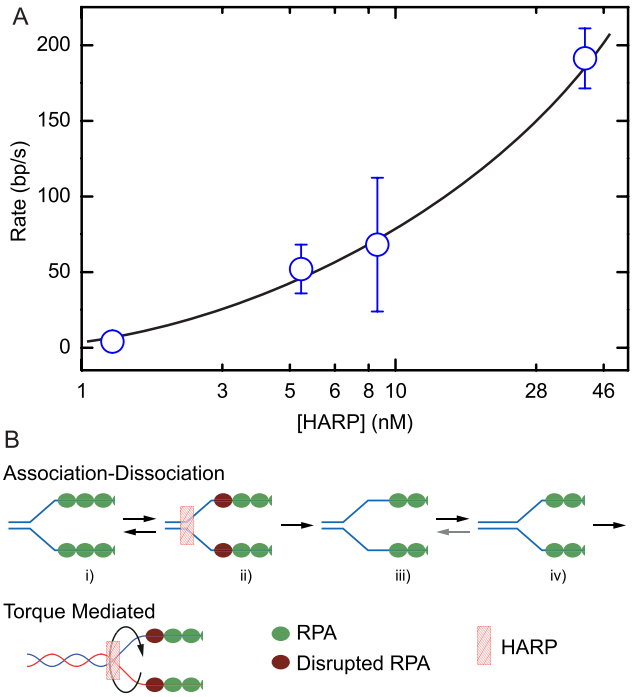

Figure 5. (**A**) The rate of bubble closure increases as a function of HARP concentration, indicating low processivity. Error bars are sem; $n = 5, 6, 5, 7$ in order of increasing concentration. (**B**) We propose that the low processive re-annealing action of HARP is due to the removal of single RPA molecules through an association-dissociation mechanism, with the protein not remaining on the substrate between RPA removals. Line is a guide to the eye.

start, for our 21 kb DNA molecule. The conclusions drawn are not affected by the number of bubbles present.

HARP has low processivity and interacts with bare DNA

The rate of a processive translocating enzyme would be expected to be independent of enzyme concentration as, once bound to the DNA substrate, the process is unaffected by free enzyme. With the relatively small size of RPA-stabilized bubbles in our assay, it thus would be expected that processive HARP action would be able to completely rewind the whole bubble. In that case, the re-annealing rate would be independent of HARP concentration, which only determines the binding on rate, k_{on}. However, as displayed in Figure 5A, this is not the case—the rate of bubble closure clearly increases with HARP concentration. The data thus indicate that the HARP enzyme has a non-processive nature, likely due to an association-dissociation mechanism where HARP does not remain on the substrate after removing single units of RPA.

We also investigated the interaction of HARP with bare DNA (i.e. without any RPA in the reaction) in both positively and negatively supercoiled states. When positively supercoiled (Supplementary Figure S5), no interaction was observed, consistent with the absence of bubbles and hence fork structures in the DNA, thus leading to no binding. Upon negative supercoiling, DNA will spontaneously form transient bubbles (4), and with the addition of HARP alone we observe intermittent interactions (Supplementary Figure S6a), attributed to single HARP interaction events. At higher HARP only concentrations these interactions become fixed 'jumps' in microsphere height (Supplementary Figures S6a and b). It has been suggested that the torque generated by a translocating Snf2 family protein may play an important role in remodeling (43) and it has been shown RPA dissociation is torque driven (27). These facts indicate two possibilities, firstly, HARP can stabilize bare DNA bubbles, and, secondly, as has already been shown for similar proteins in the Snf2 family, HARP may impart torque upon binding (17). The number of spontaneous bubbles that form in our experiments is limited due to an energy balance between hybridization and thermal fluctuations and we hypothesize that at sufficient HARP concentration, the limited number of bubbles that are formed are saturated with bubble-stabilizing HARP, such that the increase in height attains a maximum value.

DISCUSSION

A model for RPA-stabilized bubble closure

We propose a mechanism through which HARP acts to re-anneal RPA-stabilized bubbles. The steps in activity traces, attributed to RPA removal, demonstrate that the re-annealing is not a smooth process that occurs due to the gradual re-hybridization of the homologous strands but rather a consequence of the active (43,44) nature of the enzyme in disrupting the binding of RPA, and hence its removal, allowing re-hybridization. HARP must hydrolyze ATP in order to close the very stable RPA bubbles.

The slowing down of the re-annealing as a function of ionic strength and the increase in rate as a function of HARP concentration points towards a mechanism where HARP has very low processivity because it acts to remove a single RPA per interaction, which is an association-dissociation mechanism (Figure 5B). From steps (i)–(ii) HARP binds reversibly to an RPA-fork junction; in (ii) HARP disrupts RPA molecules such that they disassociate from the DNA, leaving two bare complementary strands of DNA (iii); the DNA is thus free to re-anneal and close the bubble (iv). It remains possible that between steps (i) and (iv) HARP assists in the re-annealing and in some way regulates the re-opening of the bubble. The evidence also suggests HARP may induce torque at the fork structure to disrupt the RPA molecules and that it is likely that HARP acts at both ends of a bubble simultaneously, or requires multiple units at a single fork.

CONCLUSION

Through formation of RPA-stabilized bubbles at the single-molecule level, we have been able to gain insight into the mechanism of action of HARP on a physiologically relevant substrate. We have showed that HARP closes RPA-stabilized bubbles through an association-dissociation mechanism, likely with the action of more than one enzyme simultaneously. Furthermore, our work provides insight into the structure of RPA bubbles at physiologically relevant supercoiling.The data indicate that for $\sigma \approx -0.03$ at least five bubbles exist and that the RPA molecules on

these bubbles are mis-registered on the two complementary strands. The development of this assay and this work lays the groundwork for future studies such as those investigating mutant HARP, or similar torsionally-dependent systems.

SUPPLEMENTARY DATA

Supplementary Data are available at NAR Online.

ACKNOWLEDGEMENTS

The authors would like to thank Jaco van der Torre, Bronwen Cross and Susanne Hage for DNA constructs and discussions, and Jacob Kerssemakers, David Dulin, Jan Lipfert, Marijn van Loenhout, Bojk Berghuis and Visnhu Bladew for fruitful discussions.

FUNDING

Netherlands Organisation for Scientific Research (NWO/OCW), as part of the Frontiers of Nanoscience program; European Research Council Research Grant NanoforBio [247072]; NanoNextNL. Funding for open access charge: Netherlands Organisation for Scientific Research (NWO/OCW), as part of the Frontiers of Nanoscience program; European Research Council Research Grant NanoforBio [247072]; NanoNextNL.
Conflict of interest statement. None declared.

REFERENCES

1. Lohman,T.M., Tomko,E.J. and Wu,C.G. (2008) Non-hexameric DNA helicases and translocases: mechanisms and regulation. *Nat. Rev. Mol. Cell Biol.*, **9**, 391–401.
2. Naughton,C., Avlonitis,N., Corless,S., Prendergast,J.G., Mati,I.K., Eijk,P.P., Cockroft,S.L., Bradley,M., Ylstra,B. and Gilbert,N. (2013) Transcription forms and remodels supercoiling domains unfolding large-scale chromatin structures. *Nat. Struct. Mol. Biol.*, **20**, 387–395.
3. Kouzine,F., Gupta,A., Baranello,L., Wojtowicz,D., Ben-Aissa,K., Liu,J., Przytycka,T.M. and Levens,D. (2013) Transcription-dependent dynamic supercoiling is a short-range genomic force. *Nat. Struct. Mol. Biol.*, **20**, 396–403.
4. Tempestini,A., Cassina,V., Brogioli,D., Ziano,R., Erba,S., Giovannoni,R., Cerrito,M.G., Salerno,D. and Mantegazza,F. (2012) Magnetic tweezers measurements of the nanomechanical stability of DNA against denaturation at various conditions of pH and ionic strength. *Nucleic Acids Res.*, **41**, 2009–2019.
5. Driscoll,R. and Cimprich,K.A. (2009) HARPing on about the DNA damage response during replication. *Genes Dev.*, **23**, 2359–2365.
6. Wold,M.S. (1997) Replication protein A: a heterotrimeric, single-stranded DNA-binding protein required for eukaryotic DNA metabolism. *Annu. Rev. Biochem.*, **66**, 61–92.
7. Iftode,C., Daniely,Y. and Borowiec,J.A. (1999) Replication protein A (RPA) the eukaryotic SSB. *Crit. Rev. Biochem. Mol. Biol.*, **34**, 141–180.
8. Krejci,L. and Sung,P. (2002) RPA not that different from SSB. *Structure*, **10**, 601–602.
9. Yusufzai,T. and Kadonaga,J.T. (2008) HARP is an ATP-driven annealing helicase. *Science*, **322**, 748–750.
10. Yusufzai,T., Kong,X., Yokomori,K. and Kadonaga,J.T. (2009) The annealing helicase HARP is recruited to DNA repair sites via an interaction with RPA. *Biochem. J.*, **23**, 2400–2404.
11. Yuan,J., Ghosal,G. and Chen,J. (2009) The annealing helicase HARP protects stalled replication forks. *Genes Dev.*, **23**, 2394–2399.
12. Bétous,R., Mason,A.C., Rambo,R.P., Bansbach,C.E., Badu-Nkansah,A., Sirbu,B.M., Eichman,B.F. and Cortez,D. (2012) SMARCAL1 catalyzes fork regression and Holliday junction migration to maintain genome stability during DNA replication. *Genes Dev.*, **26**, 151–162.
13. Bétous,R., Couch,F.B., Mason,A.C., Eichman,B.F., Manosas,M. and Cortez,D. (2013) Substrate-selective repair and restart of replication forks by DNA translocases. *Cell Rep.*, **3**, 1958–1969.
14. Flaus,A., Martin,D.M.A., Barton,G.J. and Owen-Hughes,T. (2006) Identification of multiple distinct Snf2 subfamilies with conserved structural motifs. *Nucleic Acids Res.*, **34**, 2887–2905.
15. Coleman,M.A., Eisen,J.A. and Mohrenweiser,H.W. (2000) Cloning and characterization of HARP/SMARCAL1: a prokaryotic HepA-Related SNF2 helicase protein from human and mouse. *Genomics*, **65**, 274–282.
16. Pazin,M.J. and Kadonaga,J.T. (1997) SWI2/SNF2 and related proteins: ATP-driven motors that disrupt protein-DNA interactions? *Cell*, **88**, 737–740.
17. Lia,G., Praly,E., Ferreira,H., Stockdale,C., Tse-Dinh,Y.C., Dunlap,D., Croquette,V., Bensimon,D. and Owen-Hughes,T. (2006) Direct observation of DNA distortion by the RSC complex. *Mol. Cell*, **21**, 417–425.
18. Manosas,M., Perumal,S.K., Bianco,P., Ritort,F., Benkovic,S.J. and Croquette,V. (2013) RecG and UvsW catalyse robust DNA rewinding critical for stalled DNA replication fork rescue. *Nat. Commun.*, **4**, 2368.
19. Yusufzai,T. and Kadonaga,J.T. (2010) Annealing helicase 2 (AH2), a DNA-rewinding motor with an HNH motif. *PNAS*, **107**, 20970–20973.
20. Boerkoel,C.F., Takashima,H., John,J., Yan,J., Stankiewicz,P., Rosenbarker,L., André,J., Bogdanovic,R., Burguet,A., Cockfield,S. *et al.* (2002) Mutant chromatin remodeling protein SMARCAL1 causes Schimke immuno-osseous dysplasia. *Nat. Genet.*, **30**, 215–220.
21. Ciccia,A., Bredemeyer,A.L., Sowa,M.E., Terret,M.-E., Jallepalli,P.V., Harper,J.W. and Elledge,S.J. (2009) The SIOD disorder protein SMARCAL1 is an RPA-interacting protein involved in replication fork restart. *Genes Dev.*, **23**, 2415–2425.
22. Treuner,K., Ramsperger,U. and Knippers,R. (1996) Replication protein A induces the unwinding of long double-stranded DNA regions. *J. Mol. Biol.*, **259**, 104–112.
23. Benedetti,F., Japaridze,A., Dorier,J., Racko,D., Kwapich,R., Burnier,Y., Dietler,G. and Stasiak,A. (2015) Effects of physiological self-crowding of DNA on shape and biological properties of DNA molecules with various levels of supercoiling. *Nucleic Acids Res.*, **43**, 2390–2399.
24. Jeon,J. and Sung,W. (2008) How topological constraints facilitate growth and stability of bubbles in DNA. *Biophys. J.*, **95**, 3600–3605.
25. Altan-Bonnet,G., Libchaber,A. and Krichevsky,O. (2003) Bubble dynamics in double-stranded DNA. *Phys. Rev. Lett.*, **90**, 138101.
26. van Loenhout,M.T.J., de Grunt,M.V. and Dekker,C. (2012) Dynamics of DNA Supercoils. *Science*, **338**, 94–97.
27. De Vlaminck,I., Vidic,I., van Loenhout,M.T.J., Kanaar,R., Lebbink,J.H.G. and Dekker,C. (2010) Torsional regulation of hRPA-induced unwinding of double-stranded DNA. *Nucleic Acids Res.*, **38**, 4133–4142.
28. Te Velthuis,A.J.W., Kerssemakers,J.W.J., Lipfert,J. and Dekker,N.H. (2010) Quantitative guidelines for force calibration through spectral analysis of magnetic tweezers data. *Biophys. J.*, **99**, 1292–1302.
29. De Vlaminck,I., Henighan,T., van Loenhout,M.T.J., Burnham,D.R. and Dekker,C. (2012) Magnetic forces and DNA mechanics in multiplexed magnetic tweezers. *PLoS One*, **7**, 1932–6203.
30. Lipfert,J., Hao,X. and Dekker,N.H. (2009) Quantitative modeling and optimization of magnetic tweezers. *Biophys. J.*, **96**, 5040–5049.
31. van Loenhout,M.T.J., Kerssemakers,J.W.J., De Vlaminck,I. and Dekker,C. (2012) Non-bias-limited tracking of spherical particles, enabling nanometer resolution at low magnification. *Biophys. J.*, **102**, 2362–2371.
32. Kruithof,M., Chien,F., de Jager,M. and van Noort,J. (2008) Subpiconewton dynamic force spectroscopy using magnetic tweezers. *Biophys. J.*, **94**, 2343–2348.
33. Patrick,S.M. and Turchi,J.J. (1999) Replication protein A (RPA) binding to duplex cisplatin-damagedDNA is mediated through the generation of single-stranded DNA. *J. Biol. Chem.*, **274**, 14972–14978.

34. Ribeck,N., Kaplan,D.L., Bruck,I. and Saleh,O.A. (2010) DnaB helicase activity is modulated by DNA geometry and force. *Biophys. J.*, **6**, 2170–2179.
35. Lee,J.B., Hite,R.K., Hamdan,S.M., Sunney Xie,X., Richardson,C.C. and van Oijen,A.M. (2006) DNA primase acts as a molecular brake in DNA replication. *Nature*, **439**, 621–624.
36. Duderstadt,K.E., Reyes-Lamothe,R., van Oijen,A.M. and Sherratt,D.J. (2014) Replication-fork dynamics. *Cold Spring Harb. Perspect. Biol.*, **6**, a010157.
37. Ribeck,N. and Saleh,O.A. (2013) DNA unwinding by ring-shaped T4 helicase gp41 is hindered by tension on the occluded strand. *PLoS One*, **8**, e79237.
38. Marko,J.F. and Neukirch,S. (2013) Global force-torque phase diagram for the DNA double helix: structural transitions, triple points and collapsed plectonemes. *Phys. Rev. E*, **88**, 062722.
39. Weiss,J.N. (1997) The Hill equation revisited: uses and misuses. *FASEB J.*, **11**, 835–841.
40. Chung,S.H. and Kennedy,R.A. (1991) Forward-backward non-linear filtering technique for extracting small biological signals from noise. *J. Neurosci. Meth.*, **40**, 71–86.
41. Leake,M.C., Chandler,J.H., Wadhams,G.H., Bai,F., Berry,R.M. and Armitage,J.P. (2006) Stoichiometry and turnover in single, functioning membrane protein complexes. *Nature*, **443**, 355–358.
42. Savitzky,A. and Golay,M.J.E. (1964) Smoothing and differentiation of data by simplified least squares procedures. *Anal. Chem.*, **36**, 1627–1639.
43. Singleton,M.R., Dillingham,M.S. and Wigley,D.B. (2007) Structure and mechanism of helicases and nucleic acid translocases. *Annu. Rev. Biochem.*, **76**, 23–50.
44. Betterton,M. and Jülicher,F. (2005) Opening of nucleic-acid double strands by helicases: active versus passive opening. *Phys. Rev. E*, **71**, 011904.
45. Kerssemakers,J.W.J., Laura Munteanu,E., Laan,L., Noetzel,T.L., Janson,M.E. and Dogterom,M. (2006) Assembly dynamics of microtubules at molecular resolution. *Nature*, **442**, 709–712.